Roles of Metal−Support Interaction in Growth of Single- and Double-Walled Carbon Nanotubes Studied with Diameter-Controlled Iron Particles Supported on MgO

Hiroki Ago,* Kazuhiro Nakamura, Naoyasu Uehara, and Masaharu Tsuji

Institute for Materials Chemistry and Engineering and Graduate School of Engineering Sciences, Kyushu University, Kasuga, Fukuoka 816-8580, and CREST, Japan Science and Technology Agency

Received: July 15, 2004; In Final Form: September 21, 2004

The catalytic growth of single- and double-walled carbon nanotubes (SWNTs and DWNTs) by chemical vapor deposition (CVD) strongly depends on the support material. Not only the presence of nanopores in the support material but also the interaction with metal particles is believed to play an important role. Here, we study the roles of the metal−support interaction by employing iron particles with a mean diameter of 9.8 nm supported on crystalline magnesia (MgO) powder. The crystalline MgO powder has a flat surface with few nanopores so that the change of the metal particle size and the growth of nanotubes can be observed with a transmission electron microscope. We found that the original iron particles became smaller during CVD and that these small particles gave SWNTs and DWNTs when reacted with methane. The decrease in the iron particle size is likely due to thermal diffusion of iron atoms into the MgO matrix, representing strong interaction between the iron particles and the MgO support. Reduction of the catalyst under a hydrogen flow at high temperature was found to suppress nanotube growth due to the increase in the particle size. The present results provide valuable information on the nanotube growth mechanism and could be applied to the diameter-controlled or large-scale synthesis of nanotubes on support materials.

Introduction

Single-walled carbon nanotubes (SWNTs) have attracted great interest, because they show unique electronic structures and optical properties which depend on the chirality as well as the diameter. High electrical and thermal conductivity, mechanical flexibility, and chemical stability of SWNTs promise various industrial applications.[1] Double-walled carbon nanotubes (DWNTs) are also attractive because they are expected to benefit from the unique properties of SWNTs and great stability of multiwalled carbon nanotubes (MWNTs).

For the synthesis of SWNTs and DWNTs, a chemical vapor deposition (CVD) method has been widely used, because CVD is applicable to large-scale synthesis as well as growth on a substrate for device fabrication. The catalytic growth of SWNTs and DWNTs requires fine metal particles with a diameter smaller than 5 nm, which act as the catalyst at high reaction temperatures, typically 700−900 °C. To prepare such fine particles, inorganic materials with a high surface area have been frequently utilized as the support material.[2−10] The support material helps to form a number of metal particles and prevents sintering at high temperatures. Two main effects should be taken into account for the growth of SWNTs and DWNTs over the supported catalysts: (i) the presence and the size of nanopores in the support, (ii) the interaction between the metal particles and the support material.

Porous materials have been extensively studied to prepare fine metal particles for use in CVD. The main concerns are preparation of a number of metal particles inside the nanopores and the control of the nanotube diameter by the diameter of the nanopores. Ciuparu et al. reported the synthesis of SWNTs with a uniform diameter over Co metal-supported MCM-41, although the reason for the large difference between the pore size of MCM-41 (2.6 and 3.3 nm) and the SWNT diameter (0.8−0.9 nm) is unclear.[9] Li et al. suggested that the diameter of DWNTs is related to the size of nanopores existing in magnesia (MgO).[10] On the contrary, Maruyama et al. reported that the diameter of SWNTs is more sensitive to the reaction temperature than the diameter of the nanopores, because the diameter distribution of SWNTs changes with temperature.[11]

In addition to the presence of nanopores, the metal−support interaction is believed to play important roles in nanotube growth, since the nanotube yield strongly depends on the support material. For example, Fe−Mo particles on alumina (Al_2O_3) produced a much higher amount of SWNTs than those grown on silica (SiO_2).[3] This was accounted for by the stronger metal−support interaction for Al_2O_3 support than SiO_2.[3] MgO is an attractive support material from the view of a large-scale synthesis of SWNTs and DWNTs, because the supported catalysts give high-quality nanotubes and MgO can be removed by relatively mild acidic treatment.[10,12−17] The metal−support interaction has been studied by using flat substrates such as Si, SiO_2, and crystals of sapphire (Al_2O_3) and MgO as a model system.[18−21] These studies have also shown that the support material significantly influences the catalytic activity of metal catalysts, suggesting the importance of the metal−support, in this case metal−substrate, interaction.

In our previous study, we reported the catalytic activity of diameter-controlled iron particles supported on *porous* MgO powder.[17] We found that iron particles with initial diameters of 4 and 10 nm produce only SWNTs and DWNTs whose diameters are 1−4 nm, regardless of the initial particle size. This result suggests that the original iron particles become

* To whom correspondence should be addressed at the Institute for Materials Chemistry and Engineering, Kyushu University. E-mail: ago@cm.kyushu-u.ac.jp.

10.1021/jp046856y CCC: $27.50 © 2004 American Chemical Society
Published on Web 11/12/2004

smaller during CVD due to the presence of the MgO support. However, it was unclear whether the presence of the nanopores or the metal−support interaction reduced the actual particle size.

The purpose of this study is to clarify the nature and roles of metal−support interaction by employing *crystalline* MgO powder with few nanopores as the support material. Iron particles with a mean diameter of 9.8 nm with a standard deviation of 1.1 nm were used as the catalyst to follow the change of the particle size on MgO. This combination of the metal and support enabled us to directly observe the change of the particle size as a function of temperature and the period of time of annealing under an Ar atmosphere. We have found that the iron particles supported on the crystalline MgO powder produced SWNTs and DWNTs above 550 °C upon reaction with methane, even though MgO has few nanopores. It has been also clarified that heat treatment in Ar or methane decreased the size of the iron particles without agglomeration, whose size is suitable for the growth of SWNTs and DWNTs. The change of the metal particle size and the following nanotube growth will be discussed in terms of the strong metal−support interaction.

Experimental Section

Materials. Iron particles were synthesized by the thermal decomposition of iron pentacarbonyl, $Fe(CO)_5$ (Kanto Chemical), in octyl ether at 287 °C in an Ar atmosphere.[17,22,23] Oleic acid was used as a surface protective reagent with a molar ratio of $Fe(CO)_5$ to oleic acid of 1:2. Thermal decomposition gave a black colloidal solution containing iron particles. The particles were purified by adding 2-propanol, followed by centrifugation of the solution. The black precipitate was redispersed in hexane.

The hexane solution was mixed with crystalline MgO powder (Kishida Chemical) with an Fe loading of 3 wt % against MgO and stirred at room temperature for 30 min. The mixed dispersion was vacuum evaporated at 71 °C for 90 min, and the resulting powder was slightly pulverized for use as the catalyst.

Reaction. For CVD growth of carbon nanotubes, the catalyst (100 mg) was set in a quartz tube of 30 mm diameter and heated to the reaction temperatures 500−800 °C with a constant heating rate of 13 °C/min under an Ar flow (300 cm^3/min (ccm)). At the reaction temperature, the Ar gas was switched to a mixture of CH_4 (20 vol %) and Ar with a total flow rate of 1300 ccm at atmospheric pressure. The reaction time was varied from 1 min to 2 h. After the reaction, the system was cooled to room temperature under an Ar flow. For some experiments, the sample was annealed at the reaction temperature under a flow of Ar or H_2 for a certain period of time (0 min, 30 min, and 2 h), followed by introduction of methane for the reaction. We call this pretreatment annealing and the period of annealing the annealing time.

To check the effects of heating the iron particles, the catalyst was heated to 500−800 °C with the same heating rate (13 °C/min) under an Ar flow. Soon after the heating temperature was reached, the furnace was shut down, letting the sample cool to room temperature under an Ar atmosphere. We call this process heat treatment of the catalyst.

Characterization. The samples were characterized by using a transmission electron microscope (JEOL 2100F or JEOL 2010FEF) with energy-dispersive X-ray (EDX) analyzers using an accelerating voltage of 200 kV. For transmission electron microscopy (TEM) measurements, the sample was directly pressed on a TEM grid to avoid the effect of the solvent and sonication, because sonication in solvent detached some iron particles from the MgO support.[17] The carbon products were characterized using Raman spectroscopy (JASCO NRS-2000) with an excitation wavelength of 514.5 nm and a laser spot size of ca. 0.1 mm.

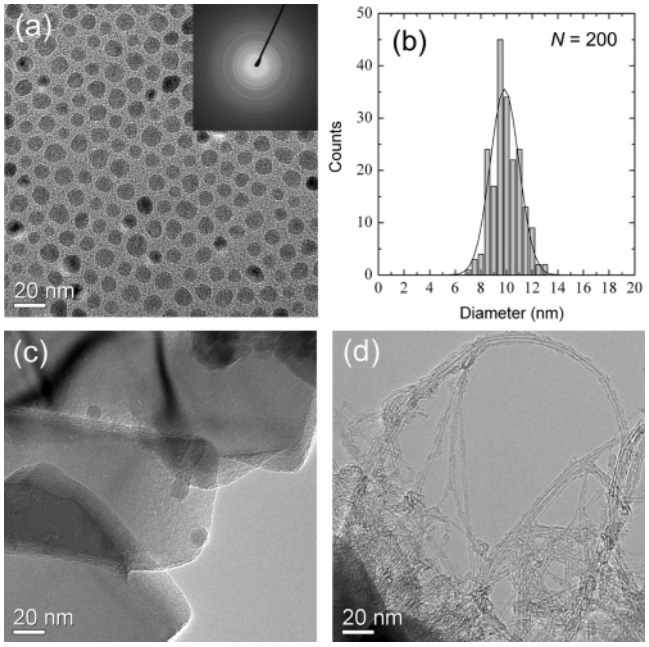

Figure 1. TEM micrograph of iron particles prepared from $Fe(CO)_5$ (a) and the electron beam diffraction pattern (inset). Size distribution of the iron particles with a Gaussian fitting curve (b). The total number of counted iron particles is 200. TEM micrographs of the iron-particle-supported MgO catalyst (c) and SWNTs grown on the catalyst under a mixture of methane (20 vol %) and Ar flow at 800 °C for 1 min (d).

Results

Catalyst Preparation and Nanotube Formation. In Figure 1a, we show the TEM image of the colloidal iron particles prepared by thermal decomposition of the $Fe(CO)_5$ precursor. The particles have a mean diameter and a standard deviation of 9.8 and 1.1 nm, respectively, as determined by a Gaussian fitting (Figure 1b). The particles prepared by the same method were reported to be Fe_2O_3 by Woo et al.[23] We also confirmed the iron particles are oxidized, but it was difficult to distinguish the Fe_2O_3 phase from Fe_3O_4 on the basis of our electron beam diffraction pattern shown in the Figure 1a inset.

The MgO supporting iron particles were also examined with a transmission electron microscope prior to the CVD reaction, as shown in Figure 1c. One can see that the MgO consists of well-defined nanocrystals with a size of several hundred nanometers. The iron particles attached on the surface of these MgO nanocrystals. Note that the present MgO nanocrystals have no clear nanopores with diameters of 1−5 nm, which differ from those studied previously.[10,17] The XRD pattern of the as-received MgO powder showed a clear diffraction pattern, indicating the present MgO is crystalline (see Figure S-1, Supporting Information). The crystalline size estimated from Scherrer's equation was 107 nm, which is close to that observed by TEM.

Figure 1d shows the TEM image of the surface of the catalyst after reacting with methane at 800 °C for 1 min. We confirmed the growth of a number of SWNTs on the MgO surface, even though the initial iron particle size was larger (10 nm) than the SWNT diameter and the reaction time was rather short (1 min). DWNTs were also found together with SWNTs, as shown later.

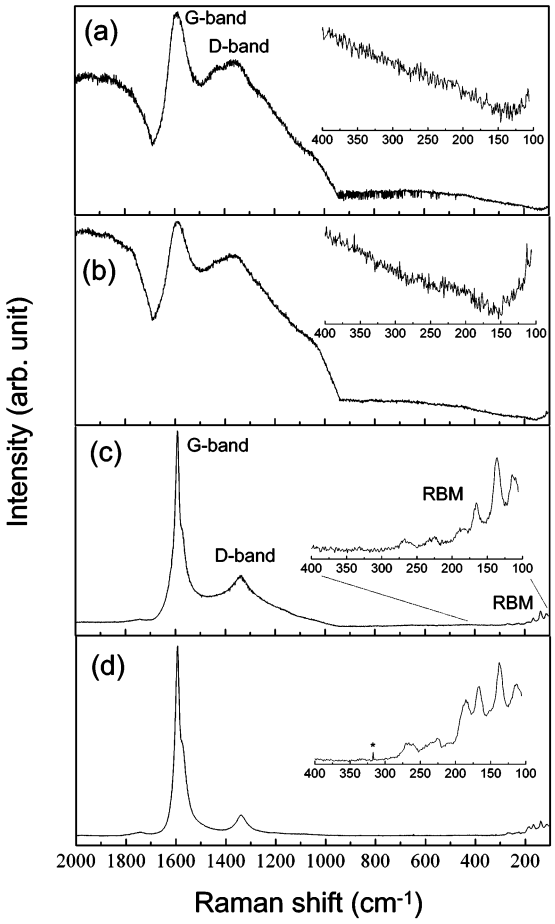

Figure 2. Raman spectra of the carbon products reacted with methane at 500 °C (a), 600 °C (b), 700 °C (c), and 800 °C (d) for 1 min. The spectra are normalized to the G-band at ca. 1589 cm^{-1}. The insets show the magnified spectra at low wavenumbers.

These results suggest that there should be characteristic interaction between the iron particles and MgO.

Temperature Dependence. Figure 2 shows the Raman spectra measured after reaction with methane at four different temperatures, 500, 600, 700, and 800 °C, for 1 min. The Raman spectra are characterized by three main signals, a G-band, a D-band, and a radial breathing mode (RBM), as indicated in Figure 2a,c. The G-band appears at around 1589 cm^{-1} and is ascribed to tangential modes of a graphene sheet. The D-band at around 1338 cm^{-1} is related to the defects in a graphene sheet and to the presence of amorphous carbon. The RBM peaks originate in carbon nanotubes with small diameters of less than 3 nm, and their position is strongly dependent on the nanotube diameter. For 1 min of reaction, no RBM peaks were observed for the samples reacted at temperatures of 500 and 600 °C (Figure 2a,b), suggesting SWNTs or DWNTs were not grown at these temperatures. This was confirmed by the corresponding TEM observations (not shown here). The strong D-band shows that the catalyst was covered with amorphous carbon together with some graphitic carbons. MWNTs were seldom observed in their TEM images, although the initial iron particle size is large enough to grow MWNTs. This is explained in terms of an insufficient carbon supply; because methane is rather stable at 500−600 °C, CVD did not produce MWNTs.

When the nanotubes were reacted at 700 °C, the growth of SWNTs and/or DWNTs was confirmed from the RBM signals as well as a strong G-band at 1589 cm^{-1} (Figure 2c). There was, however, still a strong D-band observed. The diameter of the nanotubes can be estimated from the following equation:[24]

$$\omega_r = 232/d + 6.5 \quad (1)$$

where ω_r (cm^{-1}) and d (nm) are the Raman shift of the RBM peaks and the SWNT diameter, respectively. According to this expression, the diameters of the nanotubes are calculated to be 2.15, 1.79, and 1.46 nm. The presence of thinner nanotubes is also confirmed by the relatively weak RBM signals, with estimated diameters of 1.29, 1.06, and 0.89 nm. These nanotubes are supposed to be mainly SWNTs and some DWNTs, from our TEM observations. Because the intensity of the RBM signal tends to decrease with increasing nanotube diameter, we can conclude that the present nanotubes have relatively large diameters. This may reflect the large initial diameter of the iron particles of 9.8 nm.[17]

The nanotubes reacted at 800 °C showed a Raman spectrum similar to that at 700 °C, except for the weakened D-band intensity (Figure 2d). This indicates that the higher reaction temperature is preferable for the growth of high-quality SWNTs and DWNTs. It is noted that the relative intensity of thinner nanotubes becomes stronger for the sample reacted at 800 °C compared with that reacted at 700 °C.

There was a clear difference between reaction temperatures of 600 and 700 °C. To evaluate the effects of the reaction temperature, we investigated the change in the size of the iron particles by observing heat-treated samples with a transmission electron micrscope, as shown in Figure 3. The catalyst was heated under an Ar flow to the heat-treatment temperature (500−800 °C), and soon after the temperature was reached, the furnace was shut down and cooled to room temperature, followed by collection of the catalyst for the TEM observation. Hence, the TEM image of the heat-treated sample shown in Figure 3 should reflect the actual metal size just before the methane gas is introduced. It is assumed that the dark contrast in Figure 3 corresponds to the iron particles. To check this, we performed elemental mapping of the heat-treated sample (500 °C) with a scanning transmission electron microscope and an EDX system (Figure 4). One can see that Fe is enriched at the region where the TEM image looks dark, while Mg distributes the whole catalyst. This confirms that the dark particles observed in Figure 3 consist of mainly Fe. One can see that there is some wide distribution of Fe, suggesting the possible diffusion of Fe atoms into the MgO matrix, as discussed later.

Interestingly, we observed the diameter of the iron particles became smaller at a heat-treatment temperature higher than 700 °C, as seen in Figure 3c,d. The diameters of the iron particles heated at 700 and 800 °C were 2−6 and 1.5−3 nm, respectively. The decrease in the particle diameter is closely related to the growth temperatures of SWNTs and DWNTs (Figure 2), and it can be considered that the presence of these fine iron particles is essential for the growth of SWNTs and DWNTs.

One can see that some amorphous material covers the surface of the iron particles heat-treated at 500 and 600 °C (Figure 3a,b). There are two possible assignments of the nature of this amorphous material: (i) the remaining protective reagent, oleic acid, and (ii) thermally diffused MgO. It is noted that the as-prepared iron particles on MgO shown in Figure 1c also showed the same amorphous coating on the surface of the iron particles. Hence, we speculate the amorphous material is mainly oleic acid. To confirm this, we have checked the TEM of the catalyst heat-treated in air at 500 °C. The corresponding TEM (Figure S-2, Supporting Information) showed that the iron particles are free from such amorphous material, indicating that the amorphous material was burned off in air. Therefore, the amorphous material mainly consists of oleic acid.

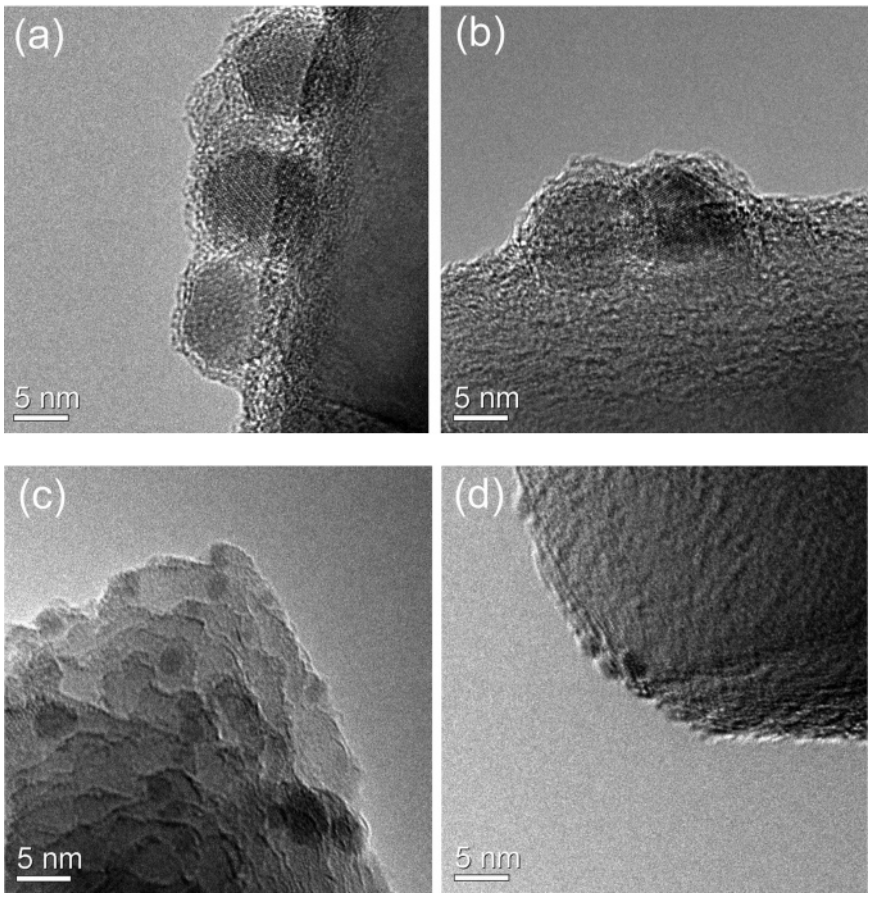

Figure 3. TEM micrographs of iron particles supported on MgO measured after heat treatment to (a) 500 °C, (b) 600 °C, (c) 700 °C, and (d) 800 °C under an Ar flow.

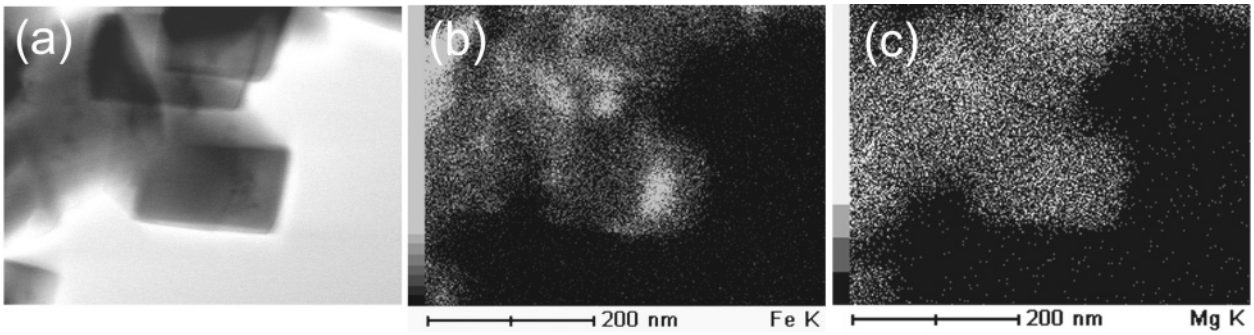

Figure 4. Scanning TEM image of the iron particles supported on MgO after heat treatment at 500 °C in Ar (a) and the corresponding elemental mapping images of Fe (b) and Mg (c) measured with an EDX system.

Annealing Effect. The heat-treatement temperature influenced the size of the iron particles when supported on MgO. In the following, we study the effects of the annealing time, period of time of maintaining the temperature before introduction of methane, on the growth of carbon nanotubes. The catalyst was set in a furnace, heated to 700 °C, and maintained for a certain period of time under Ar or H_2 (annealing time), followed by reaction with methane at the same temperature for 1 min. Figure 5a−c shows the Raman spectra of nanotubes grown at 700 °C with three different annealing times, 0 min (nonannealing), 30 min, and 5 h. One can see the increase in the RBM signals and the decrease in the D-band intensity with increasing annealing time. This result indicates that SWNT and DWNT growth was enhanced with prolonged annealing under an Ar flow. The relative peak height of the G-band to the D-band increased from 3.4 for 0 min (nonannealing) to 8.1 for 30 min of annealing.

The present results strongly suggest that Ar annealing reduced the active catalyst size to the appropriate size for SWNT and DWNT growth, which gives a higher nanotube yield with less structural defects. The relative peak intensity of the RBM peaks clearly supports this idea; the RBM peaks at higher wavenumbers (233, 225, and 268 cm^{-1}) corresponding to thinner nanotubes (1.06, 1.02, 0.89 nm) became stronger after 5 h of annealing (Figure 5c inset) compared with those of the nonannealed sample (Figure 5a inset).

Generally, catalysts are chemically reduced in the presence of hydrogen at high temperature to improve the yield. This is because hydrogen changes metal oxide particles to metal particles. We studied the effects of this reduction by treating the catalyst under a hydrogen flow at 700 °C for 30 min, followed by reaction with methane at the same temperature for 1 min. The Raman spectrum is depicted in Figure 5d. The

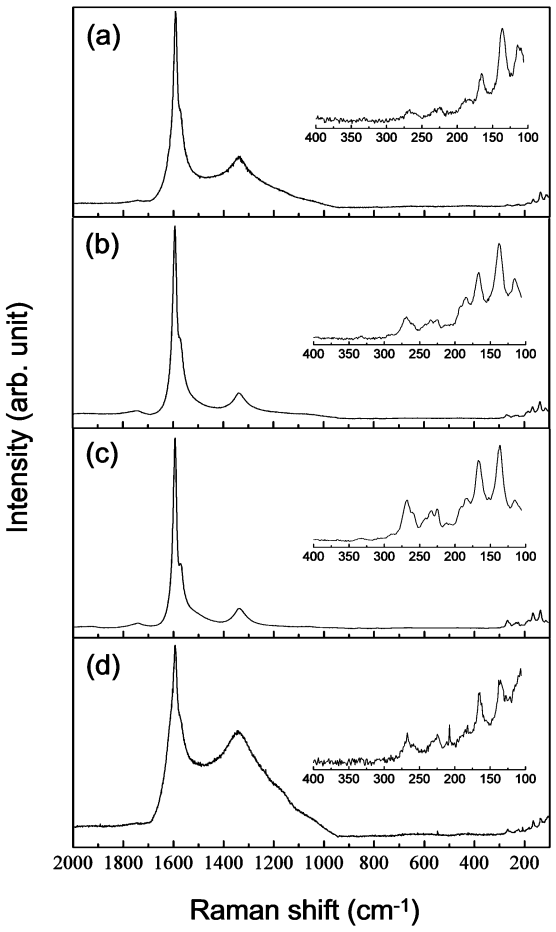

Figure 5. Raman spectra of the carbon products reacted with methane at 700 °C with different annealing times and gas flows prior to methane introduction: 0 min of annealing (methane was introduced soon after 700 °C was reached) (a), 30 min of annealing in Ar (b), 5 h of annealing in Ar (c), and 30 min of annealing in H_2 (10 vol %) with Ar (d). The reaction time with methane is 1 min for all the conditions. The insets show the magnified RBM signals.

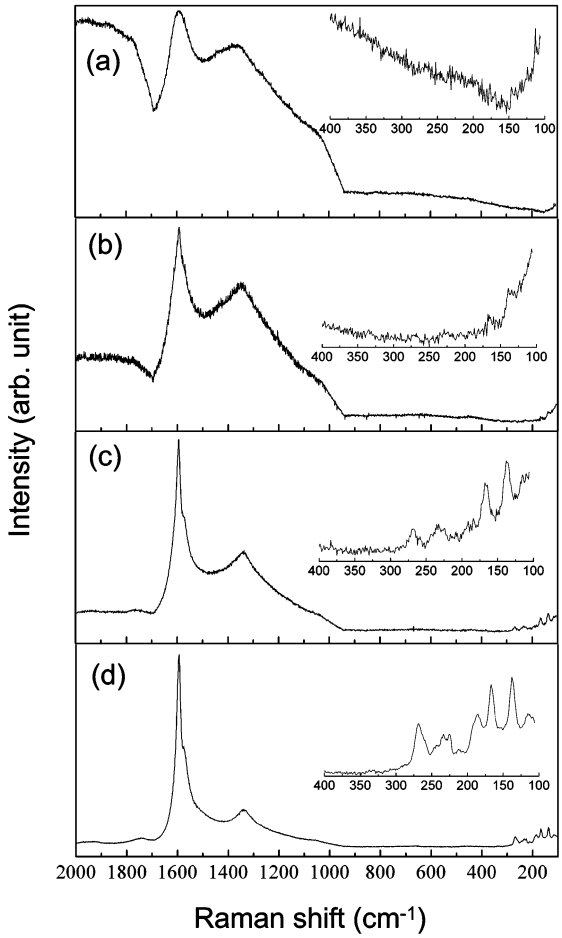

Figure 6. Raman spectra of the carbon products reacted with methane at 600 °C with different reaction times: 1 min (a), 5 min (b), 10 min (c), and 30 min (d). The insets show the magnified spectra at low wavenumbers.

reduced catalyst showed stronger D-band and weaker RBM signals compared with the sample annealed in Ar for 30 min (Figure 5b). The formation of SWNTs and/or DWNTs was found to be suppressed strongly in the presence of hydrogen. This is accounted for by the increase of the iron particle size during the reduction process, as was confirmed by the corresponding TEM image (Figure S-3, Supporting Information).

Reaction Time. No SWNTs and DWNTs were observed for the catalyst reacted with methane at 600 °C for 1 min (see Figure 2b). This may be closely related to the particle size; the size of the iron particles was essentially the same as the initial particle size so that the particles are too large to catalyze SWNT and DWNT growth (Figure 3). However, when the reaction lasted for more than 10 min, RBM signals originating in SWNTs and DWNTs appeared, as shown in Figure 6. The formation of SWNTs and DWNTs was also confirmed by TEM observation (not shown here). A close look at the RBM signals (Figure 6 inset) reveals that the longer reaction time leads to the growth of thinner nanotubes; the relative intensity of the RBM peaks of thinner nanotubes to thicker nanotubes increased for the sample after 30 min of reaction (Figure 6d) compared with that reacted for 10 min (Figure 6c). In addition to the appearance of the RBM signals, the intensity of the D-band decreased significantly as the reaction time increased. This result indicates that the original iron particles became smaller in the presence of methane, like the case of Ar annealing.[25]

It is noteworthy that SWNTs grew even at 550 °C, which is the lowest temperature reported so far.[11,26] The TEM images of the CVD product reacted at 550 °C for 2 h are shown in Figure 7. A small number of SWNTs and very short MWNTs were observed at 550 °C. No nanotube structures were seen at 500 °C. Therefore, we can say that the lowest temperature for SWNT growth is 550 °C in the present system. The observations suggest that (i) small iron particles are generated during CVD at a temperature as low as 550 °C, which catalyze the growth of SWNTs, and (ii) some remaining large particles give very short MWNTs due to the limited supply of carbon atoms because of the low reactivity of methane gas. If we use more reactive gases, such as acetylene, we may be able to get MWNTs at a low temperature. For example, Sonoda et al. synthesized MWNTs over Fe/MgO catalyst at a relatively low temperature, 600 °C, from acetylene.[27]

Discussion

We found that (i) thermal treatment in Ar or CH_4 decreases the iron particle size, (ii) SWNTs and DWNTs are formed only when the particle sizes are smaller than ca. 5 nm, and (iii) thermal treatment under H_2 suppresses nanotube growth. In the following, we discuss the growth mechanism of the nanotubes in terms of the interaction between the iron particle and the MgO support.

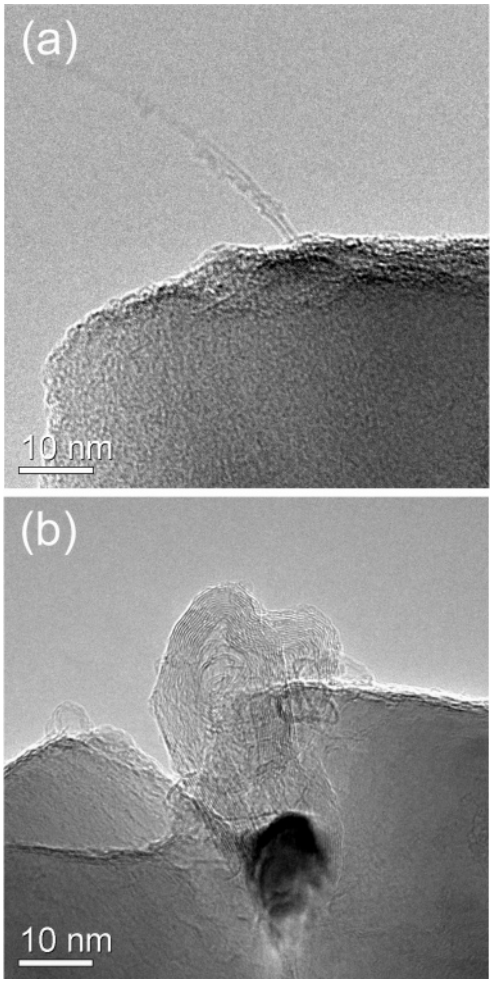

Figure 7. TEM images of an SWNT (a) and a very short MWNT grown from one large iron particle (b) obtained by reaction with methane at 550 °C for 2 h.

Growth Mechanism. Figure 8 shows the roots of carbon nanotubes synthesized at 700 °C for 1 min with methane after 30 min of annealing in Ar. Figure 8a shows a number of iron particles with diameters of 1−5 nm exist on the MgO surface, like those found in Figure 3c. Because the reaction time is relatively short, 1 min, we observed many short SWNTs together with a small amount of short DWNTs, which enabled us to observe the bases of these nanotubes. In Figure 8b, one can see that SWNTs grow from the small iron particles with diameters of 1.6 and 2.8 nm (A and B), while a large particle, 6.4 nm, gave no nanotubes (C). We could also observe the growth of a DWNT with an outer diameter of 2.1 nm from the particle with a 4.5 nm diameter, as shown in Figure 8c. As the iron particle attached to the DWNT is relatively larger than those observed for the SWNTs, it is supposed that relatively large iron particles catalyze the growth of DWNTs, while smaller ones catalyze SWNT growth. Most of the tips of the nanotubes were free from metal nanoparticles. Therefore, we believe the "base-growth" model is applied for the present catalyst, as is widely observed for SWNTs.[3,28]

Roles of Metal−Support Interaction. It is recognized that iron oxide interacts with MgO strongly. The interdiffusion phenomenon was reported by Gao et al. for the γ-Fe_2O_3 film grown on a MgO(001) substrate.[29] From Auger analyses, they found that Mg diffuses into the γ-Fe_2O_3 film when annealed at 450 °C.[29] Ruby et al. reported the formation of an Fe−Mg−O alloy phase by annealing the Fe_3O_4 thin film evaporated on the surface of a MgO crystal at 427 °C.[30] From our experimental results, we propose a growth mechanism based on the metal−support interaction, as illustrated in Figure 9. Diffusion of Fe atoms into the MgO matrix should occur in our catalyst considering the high reaction temperature of 500−800 °C. The Fe atoms in the original iron particle diffuse into the MgO matrix, probably forming an Fe−Mg−O alloy phase, resulting in a smaller particle whose size is suitable for the SWNT or DWNT growth. In addition, the strong interaction prevents the iron particles from agglomeration, which is usually observed in nanoparticles supported on flat substrates at high temperature.[31]

The chemical state of iron particles is also a very important issue. The change in the chemical state of iron particles was studied by Nishimura et al.[32] They performed an in situ X-ray diffraction (XRD) analysis during MWNT growth. Their study suggests that an iron film evaporated on a Si substrate is oxidized to Fe_2O_3 during the heating process even under a He atmosphere due to the adsorbed moisture and that introducing a hydrocarbon gas (C_2H_2) reduces the Fe_2O_3 to metallic Fe, which acts as the catalyst.[32] Arcos et al. reported metallic Fe catalyzes MWNT growth, while a less reduced iron oxide, FeO, particle is active for the growth of a thinner nanotube.[33] We cannot identify the chemical state of iron particles in our system. However, it is likely that the degree of chemical reduction of the iron particles is different for methane and hydrogen atmospheres. In particular, considering an oxygen-rich environment on the MgO support, the chemical reduction caused by the methane decomposition may be weak so that the iron particles cannot be fully reduced to iron metal. It is worthwhile to note that the reduction

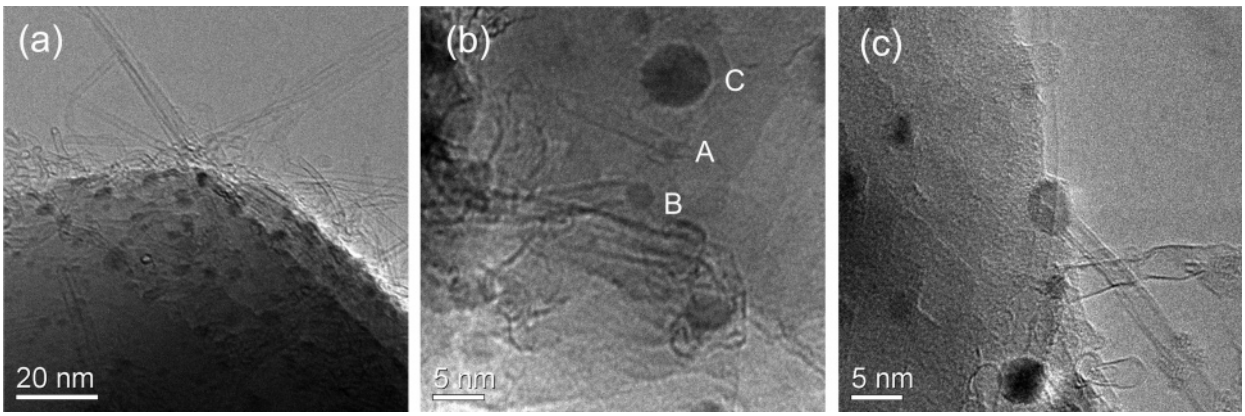

Figure 8. (a) TEM images of nanotubes grown over iron particles supported on MgO reacted at 700 °C with methane for 1 min after 30 min of annealing under Ar. (b) and (c) show the roots of two SWNTs and one DWNT, respectively. The corresponding Raman spectrum is shown in Figure 5b.

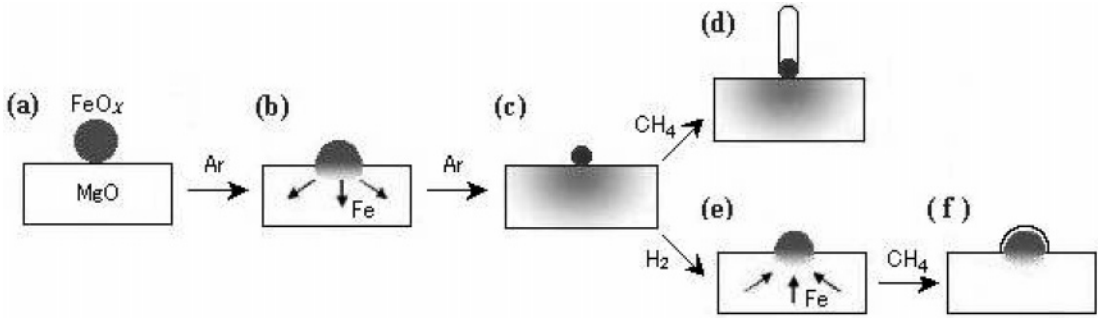

Figure 9. Proposed mechanism of SWNT formation over the iron particle supported on MgO: (a) the iron oxide particle is deposited, (b, c) heat treatment reduces the particle size due to the diffusion of iron atoms, and (d) a nanotube is formed on the nanoparticle by reaction with methane. Reduction under hydrogen causes the reprecipitation of iron particles (e), which cannot catalyze SWNT growth.

temperature of $CoAl_2O_4$ (above 900 °C), which is analogous to our Fe−Mg−O system, is much higher than that of Co_3O_4 (ca. 500 °C).[34] Therefore, it is supposed that the strong interaction between iron particles and MgO gives moderately oxidized particles suitable for the growth of SWNTs and DWNTs together with a decrease in the particle size.

Hydrogen treatment at a reaction temperature of 700 °C caused a significant increase in the D-band (see Figure 5d). This can be accounted for by the formation of larger particles than the original ones (Figure S-3, Supporting Information). Hydrogen could reduce the original iron oxide particles to reactive metallic particles, leading to agglomerated large particles. We speculate that the precipitation of dissolved Fe atoms can also occur during the hydrogen treatment (Figure 9e). It is interesting to note that solid alloys, such as Co_xMgO_{1-x} and $Fe_xCo_yMg_{0.8}Al_2O_4$, catalyzed the growth of SWNTs and DWNTs, when the catalysts were reduced under a hydrogen atmosphere.[35,36] This supports the idea that hydrogen enhances the precipitation of transition-metal nanoparticles. The CVD reaction with methane gives hydrogen due to the catalytic decomposition of methane, and the as-produced hydrogen may also help to precipitate Fe from the MgO surface. Therefore, both the diffusion of Fe atoms into the MgO matrix and the precipitation from the MgO may occur at the same time during the actual CVD growth process of SWNTs and DWNTs.

Iron salts, such as iron nitrate and iron chloride, were frequently used for the preparation of catalysts on porous support materials.[2,3,12−14] In that case, iron particles are formed during heating of the catalyst or the calcination procedure so that it is difficult to control the particle size and the size distribution precisely. We have confirmed that the iron particles formed from iron nitrate have a rather broad size distribution on the crystalline MgO powder from TEM observation (Figure S-4, Supporting Information). Our experiments showed that a longer annealing time significantly improved the crystallinity and the yield of SWNTs and DWNTs. Therefore, it is expected that adjusting the annealing time as well as the concentration of the metal salt would give a high nanotube yield and control of the particle diameter on the MgO support.

Conclusions

We have investigated the growth mechanism of SWNTs and DWNTs over an Fe/MgO catalyst. Iron particles with a mean diameter of 9.8 nm supported on MgO powder with a crystalline size of 107 nm have been studied as the catalyst. The iron particles were found to become smaller when annealed in Ar or methane, probably through thermal diffusion of Fe atoms into the MgO matrix, reflecting the strong metal−support interaction. We found that this decrease in the particle size is strongly correlated with the yield and the diameter distribution of SWNTs and DWNTs and that these nanotubes are formed on the basis of the base-growth mechanism. On the other hand, the presence of hydrogen increased the particle size and suppressed nanotube growth. Therefore, we suppose that both Fe diffusion into the MgO matrix and reverse precipitation of Fe atoms occur simultaneously in the actual CVD growth of SWNTs and DWNTs. The present result shows that nanopores are not necessary in the support material for the growth of SWNTs and DWNTs, if we can realize fine particles as small as the nanotube diameter. Our new findings would help us to develop a large-scale synthesis or diameter-controlled growth of SWNTs and DWNTs.

Acknowledgment. We acknowledge Dr. T. Setoguchi and Mr. N. Tomonaga of MHI and Dr. M. Yumura, Dr. T. Saito, and Dr. S. Ohshima of AIST for helpful discussions, and are grateful to Prof. I. Mochida of Kyushu University for the use of the Raman spectrometer and the transmission electron microscope (JEOL 2100F). The scanning TEM (JEOL 2010FE) measurements were made at the Research Laboratory for High Voltage Electron Microscopy with the assistance of Mr. Manabe. Part of this work was supported by KAKENHI (Grant No. 16710087), the Nanocarbon Technology Project of NEDO, and JST-CREST.

Supporting Information Available: XRD pattern of as-received MgO powder (Figure S-1), TEM image of the iron particles supported on MgO measured after heat treatment in air at 600 °C (Figure S-2), TEM image of the catalyst annealed under a hydrogen flow at 700 °C for 30 min, followed by reaction with methane at the same temperature for 1 min (Figure S-3), and TEM image of the iron nitrate impregnated MgO catalyst measured after heat treatment at 800 °C (Figure S-4) (PDF). This material is available free of charge via the Internet at http://pubs.acs.org.

References and Notes

(1) Tanaka, K., Yamabe, T., Fukui, K., Eds. *The Science and Technology of Carbon Nanotubes*; Elsevier: Oxford, 1999.

(2) Dai, H.; Rinzler, A. G.; Nikolaev, P.; Thess, A.; Colbert, D. T.; Smalley, R. E. *Chem. Phys. Lett.* **1996**, *260*, 471.

(3) Cassell, A. M.; Raymakers, J. A.; Kong, J.; Dai, H. *J. Phys. Chem. B* **1999**, *103*, 6484.

(4) Colomer, J.-F.; Bister, G.; Willems, I.; Konya, Z.; Fonseca, A.; Tendeloo, G. V.; Nagy, J. B. *Chem. Commun.* **1999**, 1343.

(5) Kitiyanan, B.; Alvarez, W. E.; Harwell, J. H.; Resasco, D. E. *Chem. Phys. Lett.* **2000**, *317*, 497.

(6) Su, M.; Zheng, B.; Liu, J. *Chem. Phys. Lett.* **2000**, *322*, 321.

(7) Peigney, A.; Coquay, P.; Flahaut, E.; Vandenberghe, R. E.; Grave, E. D.; Laurent, C. *J. Phys. Chem. B* **2001**, *105*, 9699.

(8) Harutyunyan, A. R.; Pradhan, B. K.; Kim, U. J.; Chen, G.; Eklund, P. C. *Nano Lett.* **2002**, *2*, 525.

(9) Ciuparu, D.; Chen, Y.; Lim, S.; Haller, G. L.; Pfefferle, L. *J. Phys. Chem. B* **2004**, *108*, 503.
(10) Li, W. Z.; Wen, J. G.; Sennett, M.; Ren, Z. F. *Chem. Phys. Lett.* **2003**, *368*, 299.
(11) Maruyama, S.; Kojima, R.; Miyauchi, Y.; Chiashi, S.; Kohno, M. *Chem. Phys. Lett.* **2002**, *360*, 229.
(12) Liu, B. C.; Lyu, S. C.; Lee, T. J.; Choi, S. K.; Eum, S. J.; Yang, C. W.; Park, C. Y.; Lee, C. J. *Chem. Phys. Lett.* **2003**, *373*, 475.
(13) Colomer, J.-F.; Stephan, C.; Lefrant, S.; Tendeloo, G. V.; Willems, I.; Konya, Z.; Fonseca, A.; Laurent, Ch.; Nagy, J. B. *Chem. Phys. Lett.* **2000**, *317*, 83.
(14) Colomer, J.-F.; Benoit, J.-M.; Stephan, C.; Lefrant, S.; Tendeloo, G. V.; Nagy, J. B. *Chem. Phys. Lett.* **2001**, *345*, 11.
(15) Yan, H.; Li, Q.; Zhang, J.; Liu, Z. *Carbon* **2002**, *40*, 2693.
(16) Jeong, H. J.; An, K. H.; Lim, S. C.; Park, M. S.; Chang, J. S.; Park, S. E.; Eum, S. J.; Ynag, C. W.; Park, C. Y.; Lee, Y. H. *Chem. Phys. Lett.* **2003**, *380*, 263.
(17) Ago, H.; Nakamura, K.; Imamura, S.; Tsuji, M. *Chem. Phys. Lett.* **2004**, *391*, 308.
(18) Ward, J. W.; Wei, B. Q.; Ajayan, P. M. *Chem. Phys. Lett.* **2003**, *376*, 717.
(19) Jung, Y. J.; Homma, Y.; Ogino, T.; Kobayashi, Y.; Takagi, D.; Wei, B.; Vajtai, R.; Ajayan, P. M. *J. Phys. Chem. B* **2003**, *107*, 6859.
(20) Arcos, T.; Vonau, F.; Garnier, M. G.; Thommen, V.; Boyen, H. G.; Oelhafen, P.; Duggelin, M.; Mathis, D.; Guggenheim, R. *Appl. Phys. Lett.* **2002**, *80*, 2383.
(21) Hongo, H.; Yudasaka, M.; Ichihashi, T.; Nihey, F.; Iijima, S. *Chem. Phys. Lett.* **2002**, *361*, 349.
(22) Cheung, C. L.; Kurtz, A.; Park, H.; Lieber, C. M. *J. Phys. Chem. B* **2002**, *106*, 2429.
(23) Woo, K.; Hong, J.; Choi, S.; Lee, H. W.; Ahn, J. P.; Kim, C. S.; Lee, S. W. *Chem. Mater.* **2004**, *16*, 2814.
(24) Alvarez, L.; Righi, A.; Guillard, T.; Rols, S.; Anglaret, E.; Laplaze, D.; Sauvajol, J. L. *Chem. Phys. Lett.* **2000**, *316*, 186.
(25) Homma, Y.; Kobayashi, Y.; Ogino, T.; Takagi, D.; Ito, R.; Jung, Y. J.; Ajayan, P. M. *J. Phys. Chem. B* **2003**, *107*, 12161.
(26) Seidel, R.; Duesberg, G. S.; Unger, E.; Graham, A. P.; Liebau, M.; Kreupl, F. *J. Phys. Chem. B* **2004**, *108*, 1888.
(27) Sonoda, Y.; Duclaux, L.; Beguin, F. *Carbon* **2002**, *40*, 965.
(28) Zhang, Y.; Li, Y.; Kim, W.; Wang, D.; Dai, H. *Appl. Phys. A* **2002**, *74*, 325.
(29) Gao, Y.; Kim, Y. J.; Thevuthasan, S.; Chambers, S. A.; Lubitz, P. *J. Appl. Phys.* **1997**, *81*, 3253.
(30) Ruby, C.; Fusy, J.; Génin, J. M. R. *Thin Solid Films* **1999**, *352*, 22.
(31) Klinke, C.; Bonard, J. M.; Kern, K. *J. Phys. Chem. B* **2004**, *108*, 11357.
(32) Nishimura, K.; Okazaki, N.; Pan, L.; Nakayama, Y. *Jpn. J. Appl. Phys.* **2004**, *43*, L471.
(33) Arcos, T.; Garnier, M. G.; Seo, J. W.; Oelhafen, P.; Thommen, V.; Mathys, D. *J. Phys. Chem. B* **2004**, *108*, 7728.
(34) Wang, W. J.; Chen, Y. W. *Appl. Catal.* **1991**, *77*, 223.
(35) Bacsa, R. R.; Laurent, Ch.; Peigney, A.; Bacsa, W. S.; Vaugien, Th.; Rousset, A. *Chem. Phys. Lett.* **2000**, *323*, 566.
(36) Flahaut, E.; Govindaraj, A.; Peigney, A.; Laurent, Ch.; Rousset, A.; Rao, C. N. R. *Chem. Phys. Lett.* **1999**, *300*, 236.